Nonisolated ZVT Two-Inductor Boost Converter With a Single Resonant Inductor for High Step-Up Applications

Kui-Jun Lee, Byoung-Gun Park, Rae-Young Kim, *Member, IEEE*, and Dong-Seok Hyun, *Fellow, IEEE*

***Abstract*—The interleaved operation of a two-inductor boost converter system is a very attractive solution for converting the low input voltage (30–50 V) of distributed power sources, such as photovoltaic and fuel cells, to the high output voltage (380–760 V) required in grid-connected power-conversion applications. However, a soft-switching method is required in the two main switches to increase the overall power conversion efficiency. This paper proposes a zero-voltage-transition (ZVT) two-inductor boost converter using a single resonant inductor to meet these needs. To satisfy the requirement of soft switching in the two main switches, a resonant cell is constructed at the output side with a bidirectional switch, two auxiliary diodes, and a single resonant inductor. This converter has the advantages of simple circuitry, reduced size, and low cost due to a single resonant inductor. The validity of the proposed ZVT two-inductor boost converter is verified through experimental results.**

***Index Terms*—Boost converter, interleaved, resonant, two-inductor, zero-voltage transition (ZVT).**

I. Introduction

As the demand for distributed generation (DG) has increased, single-phase grid-connected power conversion systems have been widely studied in order to connect distributed sources, such as photovoltaic and fuel cells, with grids [1], [2].

These power systems are commonly constructed in two stages, which can be divided into the dc–dc converter, which boosts a low voltage of 30–50 V to a high voltage of 380 V, and the dc–ac inverter for connection to the 220-V ac voltage [3]. As a rule, a full-bridge or half-bridge topology-based hard-switching inverter is applied for dc–ac inverters, while various topologies, such as nonisolated/isolated and voltage-/current-source types, have been proposed to satisfy a high step-up voltage gain for dc–dc converters.

Therefore, the dc–dc converter naturally uses the boost topology, and moreover, additional magnetic integrated topologies have been developed by considering the tradeoff of increased cost for a sufficiently high-voltage output and improved stability due to the galvanic isolation.

Boost topology with coupled inductors has been proposed for nonisolated converters [4]–[6], where the secondary winding of the coupled inductor serves as a voltage source in series with the power branch. On the other hand, a two-inductor boost converter has been developed for the isolated type [7]. Furthermore, a boost converter with a hybrid structure that combines a coupled inductor and a transformer has been attempted [8]–[11].

Among these topologies, the two-inductor boost converter has inherent characteristics that are useful for high step-up converters in DG systems. Since this type of converter has a large input current, the input current distributed by the two power branches reduces the conduction losses of the power devices and the copper losses of the inductors. Moreover, the input current ripple can be reduced by applying an interleaved control scheme that decreases the input filter size. This reduction is also very desirable in DG applications, in which the distributed sources should always be operated at the maximum power point (MPP). Since current ripples at the MPP result in power losses, the reduction of input current ripples at the dc–dc converter can maximize allowable power utilization.

However, the interleaved control-based two-inductor boost converter is characterized by switching losses and diode reverse-recovery losses that limit the switching frequency. Furthermore, switch voltage stress at turn-off increases because of the resonant phenomenon between the leakage inductance of the transformer and the parasitic capacitance of the switch.

In order to overcome these drawbacks, the two-inductor boost converter has been operated in the discontinuous conduction mode (DCM) or in boundary conduction mode (BCM) [12], [13], while the soft-switching scheme is applied in the continuous conduction mode (CCM) [14]–[17]. However, the variable operating frequencies that are the characteristic of the DCM or BCM make the filter design difficult, and the peak current, therefore, increases. Similarly, in the CCM, the switching frequency should be varied to produce variable output voltage under different load and input voltage conditions. Therefore, in [18], a two-inductor boost converter with an auxiliary transformer was attempted in order to achieve output-voltage regulation from full load to no load over a wide input voltage range using a constant switching frequency.

A zero-voltage-transition (ZVT) interleaved boost converter that operates in the CCM with a fixed switching frequency was proposed by using a resonant cell [19]. However, it is not suitable for DG applications because a resonant cell located at the input

Manuscript received February 24, 2011; revised April 26, 2011; accepted August 16, 2011. Date of current version February 20, 2012. This paper was presented at the 8th International Conference on Power Electronics (ICPE 2011-ECCE Asia), Jeju Island, Korea, May 30–June 3, 2011. Recommended for publication by Associate Editor H. S. H. Chung.

K.-J. Lee, R.-Y. Kim, and D.-S. Hyun are with the Department of Electrical Engineering, Hanyang University, Seoul 133-791, Korea (e-mail: exkjule@hanyang.ac.kr; rykim@hanyang.ac.kr; dshyun@hanyang.ac.kr).

B.-G. Park is with Korea Electrotechnology Research Institute, Changwon-si, 642-120, Korea (e-mail: bgpark@keri.re.kr).

Digital Object Identifier 10.1109/TPEL.2011.2165970

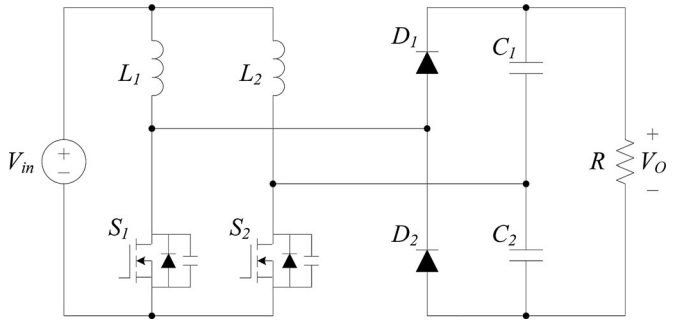

Fig. 1. Conventional two-inductor boost converter.

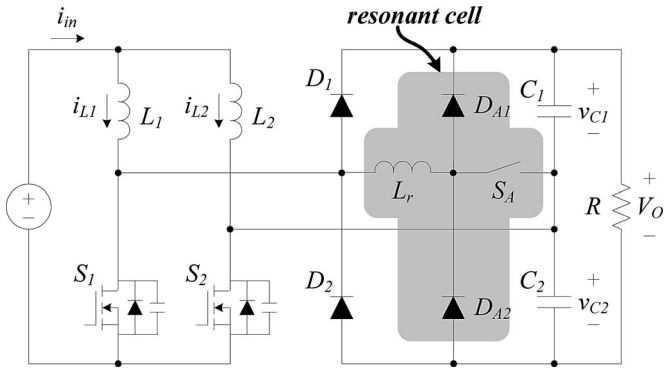

Fig. 2. Proposed nonisolated ZVT two-inductor boost converter with a single resonant inductor.

side causes increased input current ripple corresponding to the resonant current.

Therefore, this paper proposes a novel nonisolated ZVT two-inductor boost converter for high step-up applications. The zero-voltage-switching (ZVS) turn-on of the main switches is fulfilled through the resonant cell, which consists of a single resonant inductor, one bidirectional switch, and two auxiliary diodes, and the reverse-recovery losses of the rectifier diodes are eliminated by the slope control at turn-off. Furthermore, the resonant current does not perturb the input current shape since the resonant cell is located at the output side. The experimental results for a prototype 300-W ZVT two-inductor boost converter are provided to verify the effectiveness of the proposed converter.

II. Proposed Converter and Operational Principle

A. Circuit Configuration

Fig. 1 shows a conventional two-inductor boost converter. The input side is comprised of two inductors L_1 and L_2 and two main switches S_1 and S_2. The output side includes two rectifier diodes D_1 and D_2, and two output capacitors C_1 and C_2, which constitutes a voltage-doubler rectifier to obtain a high step-up voltage gain. Therefore, the output voltage V_o increases two times more than the basic single pulse width modulation boost converter.

Although the voltage balance of the voltage-doubler rectifier should be considered, it can provide twice as much boost than a full-bridge rectifier. Furthermore, if the transformer is used between the input and the output side for galvanic isolation, it can decrease the transformer turn ratio. Considering the direct relationship between the transformer's turns and the leakage inductance of the transformer, it can reduce the leakage inductance of the transformer, thereby reducing the resonant phenomenon at turn-off of the main switch.

Fig. 2 shows the proposed ZVT two-inductor boost converter, which consists of a conventional nonisolated two-inductor boost converter and a resonant cell. The resonant cells are comprised of a single resonant inductor L_r, one bidirectional switch S_A, and two auxiliary diodes D_{A1} and D_{A2}.

In order to simplify the analysis of the operational modes, L_1, L_2, C_1, and C_2 have been replaced by current and voltage sources, respectively, as shown in Fig. 3, under the following assumptions.

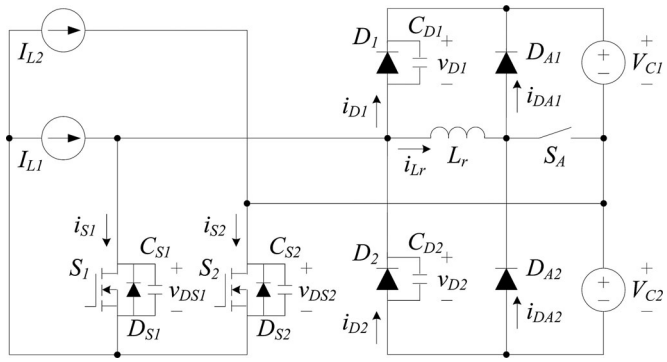

Fig. 3. Simplified circuit diagram.

1) Inductors L_1 and L_2 have large inductance values and their currents are identical constants, i.e., $I_{L1} = I_{L2}$.
2) Capacitors C_1 and C_2 are large enough to neglect the voltage ripple and their voltages are identical constants, i.e., $V_{C1} = V_{C2}$.
3) Main switches S_1 and S_2 are ideal except for the output capacitors C_{S1} and C_{S2} and the diodes D_{S1} and D_{S2} are the antiparallel diodes of S_1 and S_2, respectively. The capacitors C_{S1} and C_{S2} are the sum of the parasitic capacitors of the main switches and external added capacitors.
4) Rectifier diodes D_1 and D_2 are ideal except for the output capacitors C_{D1} and C_{D2}.
5) Capacitors C_{S1} and C_{S2} are considerably larger than the capacitors C_{D1} and C_{D2}.

B. Mode Operation

Fig. 4 shows the operational modes during the half switching period, and Fig. 5 shows the theoretical waveforms of the proposed converter during the one switching period T_s. There are 14 total modes for a single switching period. However, due to the symmetrical operation of the proposed converter, only the seven leading modes are analyzed.

1) *Mode 1* (t_0–t_1): Prior to t_0, switch S_1 turns OFF and switch S_2 turns ON. Therefore, the energy stored in inductor L_1 is transferred to the load through diode D_1, and the current of switch S_2 (i.e., i_{S1}) is the sum of I_{L1} and I_{L2}. At t_0, switch S_A turns ON, and the resonant current i_{Lr} ramps up

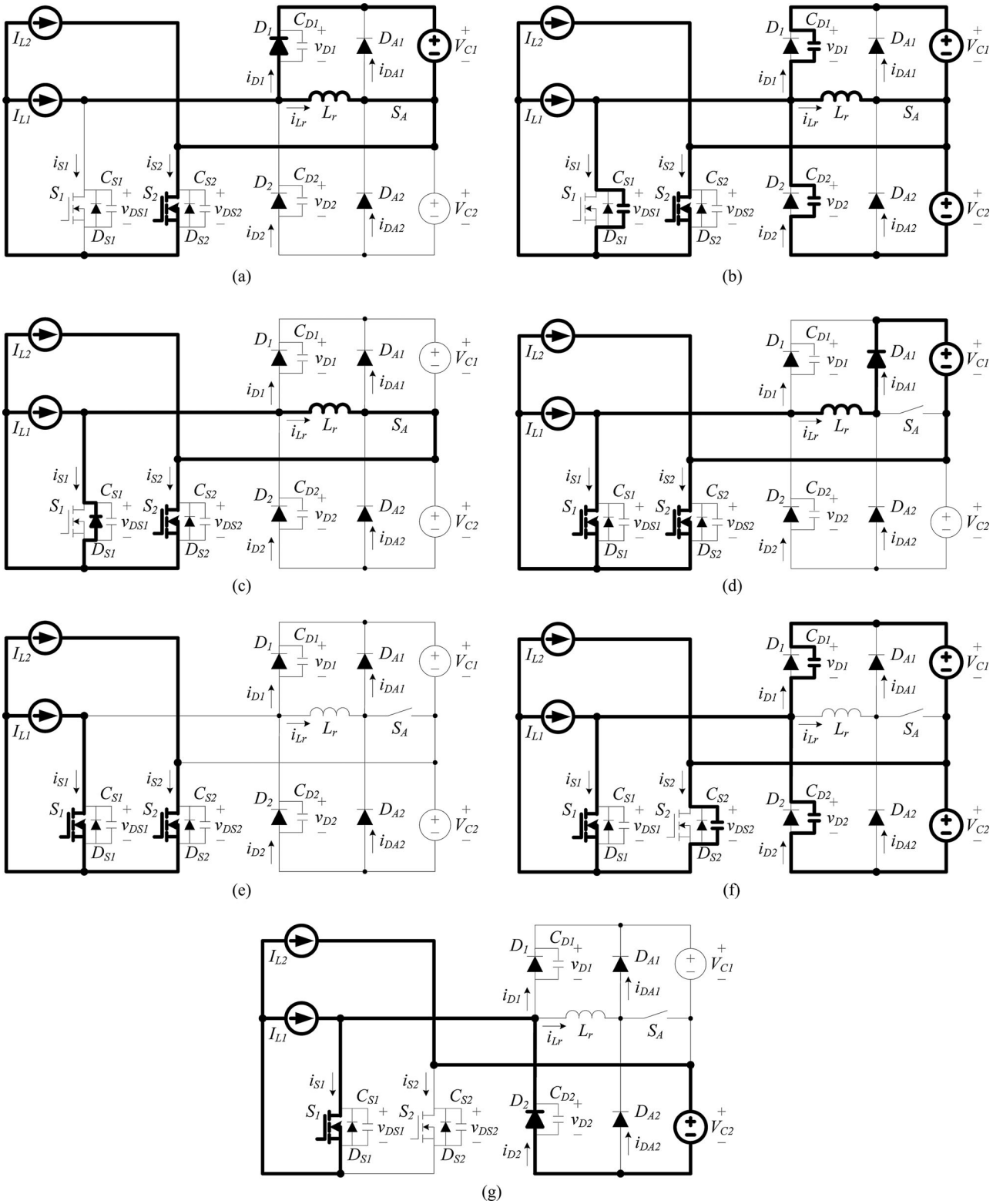

Fig. 4. Equivalent circuits for each operational mode: (a) Mode 1. (b) Mode 2. (c) Mode 3. (d) Mode 4. (e) Mode 5. (f) Mode 6. (g) Mode 7.

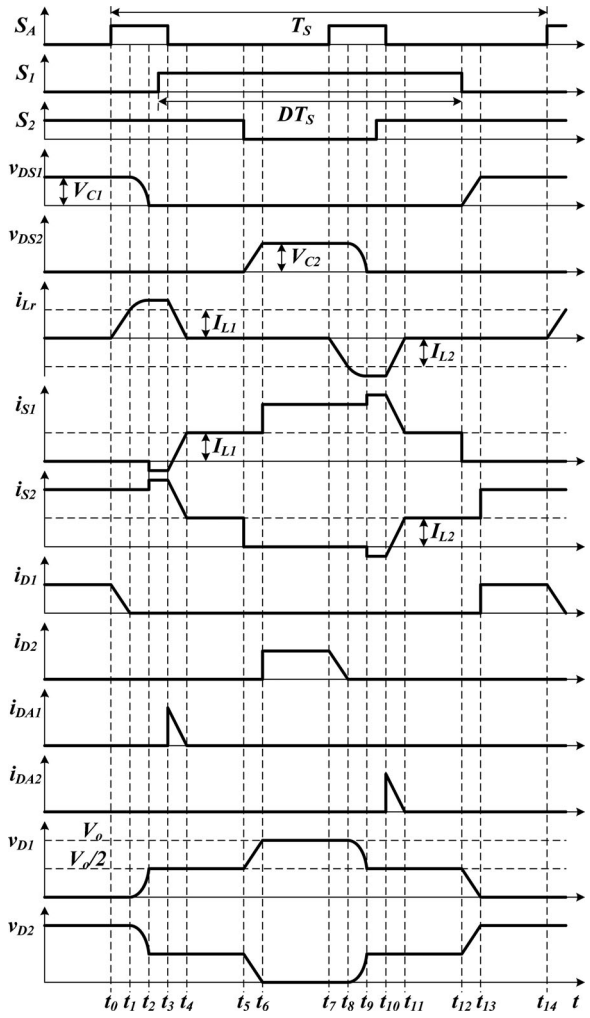

Fig. 5. Theoretical waveforms of the proposed converter.

linearly until it reaches I_{L1} at a slope of V_{C1}/L_r. During this time, the current of diode D_1 decreases linearly to zero, and it turns OFF softly with a zero-current-switching (ZCS) condition. The required time in this mode is

$$t_{01} = \frac{I_{L1}}{V_{C1}/L_r}. \tag{1}$$

2) *Mode 2* (t_1–t_2): The current i_{Lr} continues increasing because of the resonance of L_r, C_{S1}, C_{D1}, and C_{D2}. At this time, the voltage v_{DS1} decreases to zero, and diode D_{S1} begins to conduct. The resonant time is

$$t_{12} = \frac{\pi}{2}\sqrt{L_r C_r} \tag{2}$$

where $C_r = C_{S1} + C_{D1} + C_{D2}$.

3) *Mode 3* (t_2–t_3): While the current i_{S1} flows negatively through diode D_{S1}, the gating signal of switch S_1 is applied, thus satisfying the ZVS turn-on. The time delay T_d between S_A and S_1 can be obtained as

$$T_d \geq t_{01} + t_{12} = \frac{I_{L1}}{V_{C1}/L_r} + \frac{\pi}{2}\sqrt{L_r C_r}. \tag{3}$$

At this time, the current i_{S2} flows more than the sum of I_{L1} and I_{L2} because of the added resonant current.

4) *Mode 4* (t_3–t_4): Switch S_A turns OFF and the energy stored in inductor L_r is discharged through diode D_{A1}. The current i_{Lr} decreases linearly to zero, the current i_{S1} increases to I_{L1}, and the current i_{S2} decreases to I_{L2}. In this mode, the required time can be obtained as

$$t_{34} = \frac{I_{Lr\_\mathrm{peak}} L_r}{V_{C1}} \tag{4}$$

where I_{Lr_peak} is the maximum value of the resonant current.

5) *Mode 5* (t_4–t_5): The diode D_{A1} turns OFF and it operates as the charging mode of the basic boost converter.
6) *Mode 6* (t_5–t_6): The switch S_2 turns OFF and capacitor C_{S2} is linearly charged. Furthermore, capacitors C_{D1} and C_{D2} are linearly charged and discharged, respectively.
7) *Mode 7* (t_6–t_7): The voltage v_{DS2} becomes V_{C2}, and the energy stored in inductor L_2 is transferred to the load through diode D_2. It operates identically as the discharging mode of the basic boost converter.

The other half operational modes from 8 to 14 are symmetric with the aforementioned modes.

C. Design Guide of Resonant Components L_r and C_r

The value of inductor L_r is selected to minimize the reverse-recovery effects of D_1 and D_2. Specifically, the rising slope of i_{Lr} is appropriately selected, thus achieving the ZCS turn-off of D_1 and D_2. In this paper, the rising time of i_{Lr} from 0 to I_{L1} or I_{L2} is chosen to be twice the reverse-recovery time t_{rr} of D_1 or D_2. From (1), the value of L_r is given by

$$L_r = \frac{2t_{rr}V_{C1}}{I_{L\_\min}} \tag{5}$$

where $I_{L\_\min}$ is the minimum value of the boost inductor current.

Afterward, the value of capacitor C_r is selected in order to ensure soft switching even in the worst case. In Mode 2, the maximum resonant current I_{Lr_peak} is given by

$$I_{Lr\_\mathrm{peak}} = I_{L1} + \frac{V_{C1}}{Z_r}$$

$$Z_r = \sqrt{\frac{L_r}{C_r}}. \tag{6}$$

The current I_{Lr_peak} should be sufficiently large to achieve ZVS of the main switches and the resonant capacitor C_r limits the main switch's *dv/dt* at turn-off. Therefore, a relatively large resonant capacitor is desirable. However, a large capacitor can create additional switch losses and an increased resonant period so it should be appropriately restricted. In this paper, the current I_{Lr_peak} is limited to $1.2 \times I_{L1}$ and the resonant capacitance is obtained as follows from (6)

$$C_r = \frac{L_r(I_{Lr\_\mathrm{peak}} - I_{L1})^2}{V_{C1}^2}. \tag{7}$$

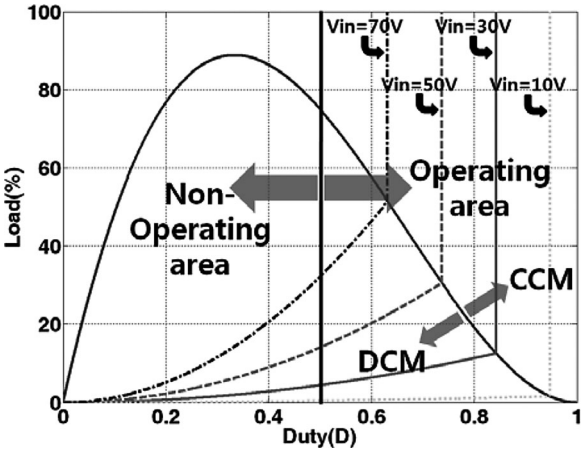

Fig. 6. Operational limitation for the 300-W prototype with $V_o = 380$ V and $T_S = 25\ \mu$s.

D. Operational Limitations

Fig. 6 shows the required duty cycle according to the load variation when a 300-W two-inductor boost converter operates to regulate a 380-V output voltage with a 40-kHz switching frequency.

The boundary load of the boost converter to differentiate between the CCM and the DCM is calculated as

$$R_e = \frac{2L}{T_S D(1-D)^2} \tag{8}$$

and the load within the DCM is presented as follows [20]:

$$R_{\mathrm{DCM}} = \frac{2L}{T_S D^2} \cdot \frac{V_o^2 - V_o V_{\mathrm{in}}}{V_{\mathrm{in}}^2} \tag{9}$$

This can be represented as a percentage of the base impedance R_{base}

$$\mathrm{Load}(\%) = \frac{R_{\mathrm{base}}}{R_{\mathrm{DCM}}} \times 100$$
$$R_{\mathrm{base}} = \frac{V_o^2}{P_o} \tag{10}$$

where P_o is the rated output power.

As shown in Fig. 6, the boost converter operates with the CCM in full load regardless of the input voltage and the duty cycle is constant within the CCM region regardless of the load variation. Furthermore, the boost converter operates with the DCM in light load, and the more the input voltage increases at a low voltage ($<$100 V), the more likely that it goes into the DCM. However, since the two-inductor boost converter should have a structural minimum of a 0.5 duty cycle for safe operation with the CCM, this limitation results in a limited operational area above a 0.5 duty cycle, as shown in Fig. 6. In the proposed soft-switching scheme, the minimum duty cycle should increase more than 0.5 $+ t_{34}/T_s$ because the one main switch should maintain the turn-on state until the resonant current i_{Lr} decreases to zero after the other main switch is softly turned ON. Therefore, the voltage regulation cannot be achieved with a light load, and the variable frequency control is required to overcome the problem.

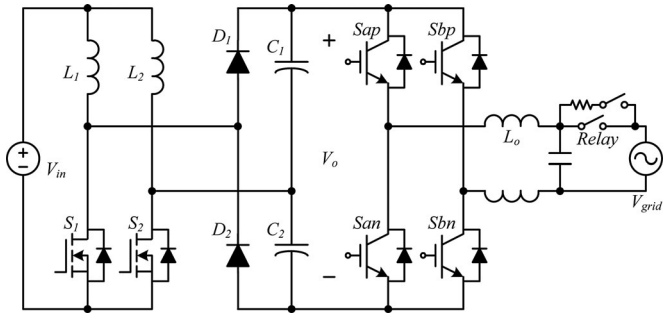

Fig. 7. Implementation of a microinverter with the two-inductor boost converter and full-bridge inverter.

E. Start-Up Issue

As mentioned earlier, the two-inductor boost converter should have a minimum 0.5 duty cycle for stable operation, and this leads to the difficult start-up for the two-inductor boost converter. Since the output voltage V_o is zero before the circuit starts up, the inrush current may damage the semiconductor devices if the gating signal is applied.

To overcome this problem, several start-up schemes by the initial precharging circuit of the output capacitor have been proposed [9], [21]. In [9], the additional winding was added within an integrated magnetic to form a push–pull circuit, and the identical gating signals were applied at the two main switches to charge the output voltage. Furthermore, this additional winding provides current path at the occasional duty cycle error $D < 0.5$ for protective purpose. In [21], a flyback transformer was formed by an additional winding within the boost inductor, and two start-up methods are proposed. While a flyback circuit charges the output voltage through the identical gating signals, the combination of boost and flyback converter achieves the precharging of the output capacitor through the interleaved control.

However, the other precharging mechanism is possible without the additional winding when the two-inductor boost converter is applied in the single-phase grid-connected power-conversion systems. Fig. 7 shows one example of a microinverter that the full-bridge inverter follows the two-inductor boost converter. While all gating signals turn OFF, the relay connected in series with resistance is closed. Therefore, the output voltage V_o reaches about the peak grid voltage through the antiparallel diodes of the inverter switches.

III. Experimental Results

To verify the theoretical operation and evaluate the performance of the proposed converter, a 300-W two-inductor boost converter prototype was designed. IRFB4332PbF MOSFETs ($V_{DS} = 250$ V, I_D@25 °C $= 60$ A, $R_{DS(\mathrm{ON})} = 0.029$ Ω) from IR was used for the main switches S_1 and S_2, and MSR1560 diodes ($V_{\mathrm{RRM}} = 600$ V, $I_O = 15$ A, $t_{rr} = 45$ ns) from Onsemi were used for the rectifier diodes D_1 and D_2.

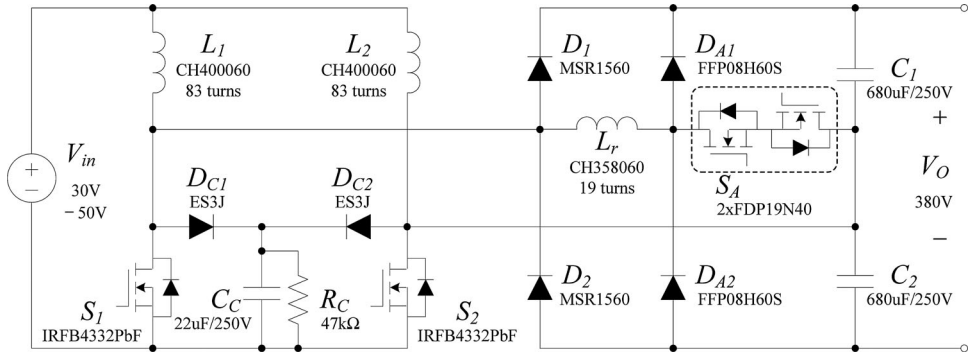

Fig. 8. Schematic diagram of the 300-W ZVT two-inductor boost converter.

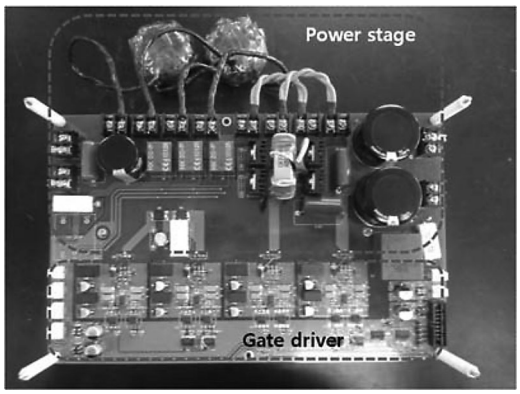

Fig. 9. Photograph of the experimental prototype.

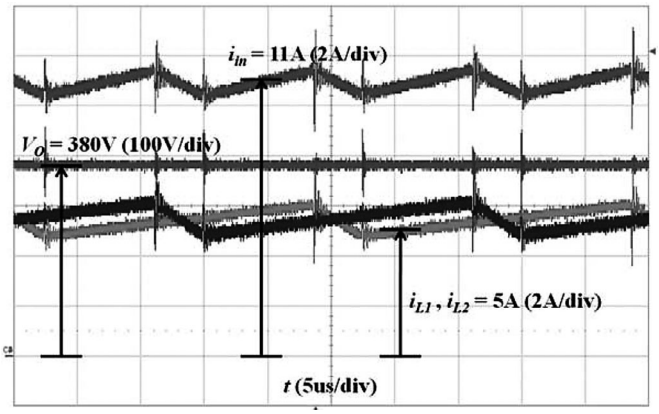

Fig. 10. Total input current waveform $i_{\rm in}$ ($=i_{L\,1}\,+\,i_{L\,2}$), boost inductor current waveforms $i_{L\,1}$ and $i_{L\,2}$, and output voltage waveform V_o at $V_{\rm in}$ = 30 V and P_o = 300 W.

TABLE I
EXPERIMENTAL CONDITIONS

Output Power (P_o)	300 W
Input Voltage (V_{in})	30 V ~ 50 V
Output Voltage (V_o)	380 V
Switching Frequency	40 kHz
Boost Inductor (L_1, L_2)	500 μH
Resonant Inductor (L_r)	21 μH

To construct the resonant cell, two FDP19N40 MOSFETs (V_{DS} = 400 V, I_D @25 °C = 19 A, $R_{DS(ON)}$ = 0.2 Ω) from Fairchild were connected in an antiparallel configuration and used for the bidirectional switch S_A, and FFP08H60S diodes ($V_{\rm RRM}$ = 600 V, I_O = 8 A, t_{rr} = 45 ns) from Fairchild were used as the auxiliary diodes $D_{A\,1}$ and $D_{A\,2}$. An additional RCD snubber circuit across the main switch was used to prevent voltage stress at turn-off. Fig. 8 shows a schematic diagram of the 300-W ZVT two-inductor boost converter, and Fig. 9 shows a photograph of the experimental prototype. The other experimental conditions are summarized in Table I.

Fig. 10 shows the steady-state waveforms of the input current and output voltage. Although each boost inductor current, i.e., $i_{L\,1}$ and $i_{L\,2}$ operates at a 40-kHz switching frequency, the total input current operates at 80 kHz, and the ripple is reduced due to the interleaved operations.

Figs. 11 and 12 show the ZVS waveforms of the main switch S_1 at a 100% load for $V_{\rm in}$ = 30 V and $V_{\rm in}$ = 50 V, respectively. As shown in Figs. 11(b) and 12(b), which are magnifications of the original waveforms, the main switch is softly turned ON.

Fig. 13 shows the operational waveforms under light load conditions. As shown in Fig. 13(a), the ZVS waveform is confirmed until 5% load under $V_{\rm in}$ = 30 V conditions. However, under $V_{\rm in}$ = 50 V conditions, the ZVS waveform is confirmed until 20% load, since the duty cycle is limited by the minimum value of 0.5 for safe operation as shown in Fig. 6. Below this duty cycle, the output voltage increases beyond 380 V due to the DCM operation.

The efficiency of the prototype was measured as shown in Fig. 14. The overall efficiency is increased through the ZVS operation of the main switches. Specifically, the efficiency increased more under $V_{\rm in}$ = 30 V conditions compared with $V_{\rm in}$ = 50 V conditions, since the magnitude of the input current is larger at $V_{\rm in}$ = 30 V for the same output power. Furthermore,

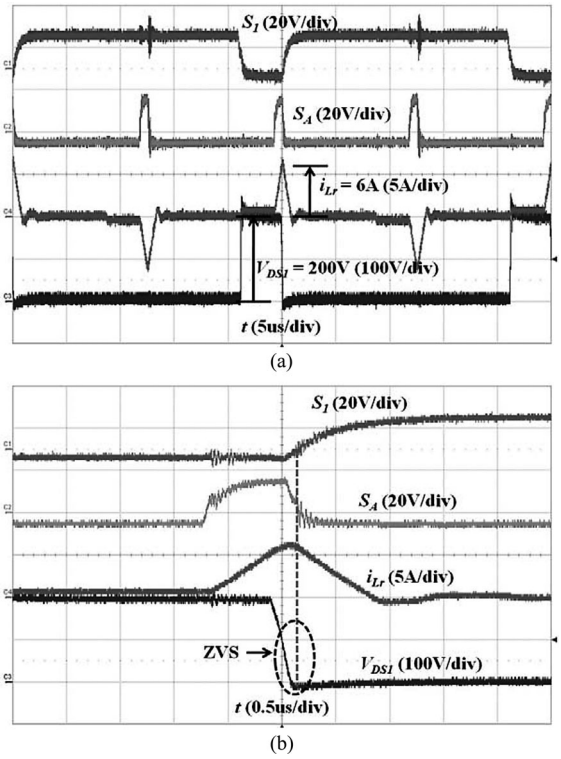

Fig. 11. Gate-to-source voltage waveforms of the main switch S_1 and the bidirectional switch S_A, resonant current waveform i_{Lr}, and drain-to-source voltage waveform of S_1 V_{DS1} at $V_{\rm in} = 30$ V and 100% load. (a) Original waveforms. (b) Magnified waveforms of (a).

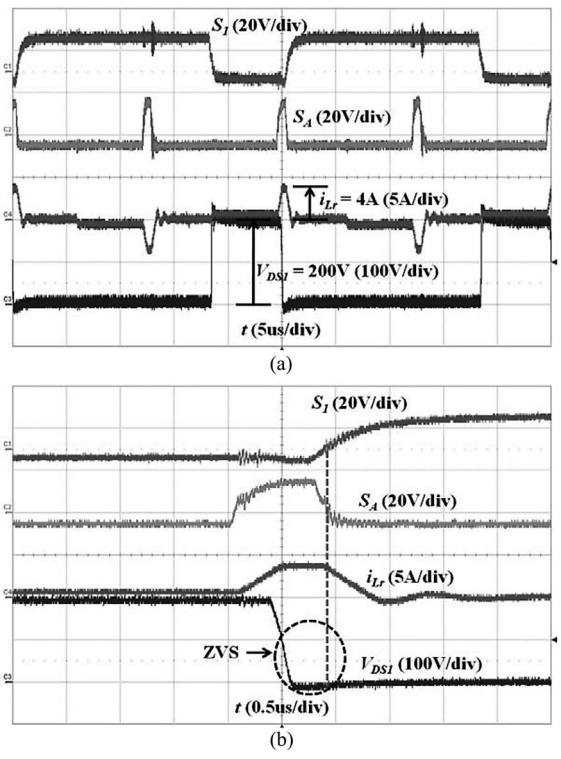

Fig. 12. Gate-to-source voltage waveforms of the main switch S_1 and the bidirectional switch S_A, resonant current waveform i_{Lr}, and drain-to-source voltage waveform of S_1 V_{DS1} at $V_{\rm in} = 50$ V and 100% load: (a) original waveforms and (b) magnified waveforms of (a).

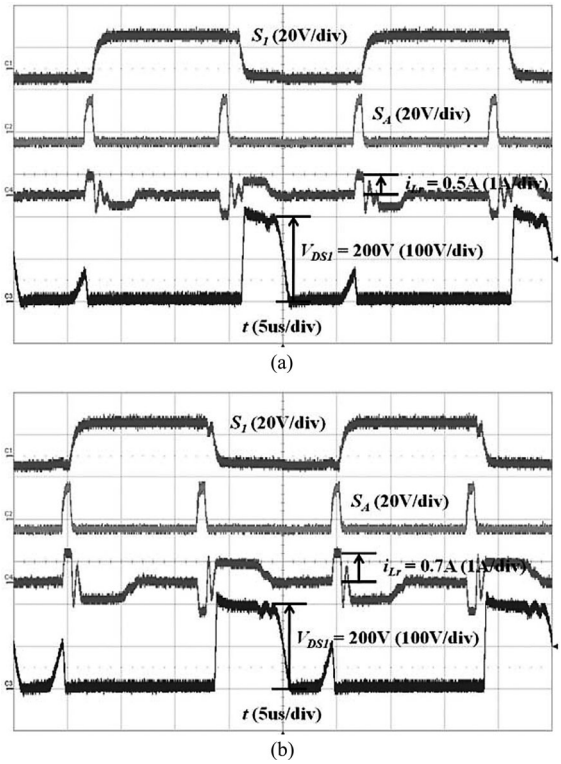

Fig. 13. Gate-to-source voltage waveforms of the main switch S_1 and the bidirectional switch S_A, resonant current waveform i_{Lr}, and drain-to-source voltage waveform of S_1 V_{DS1} at (a) $V_{\rm in} = 30$ V and 5% load and (b) $V_{\rm in} = 50$ V and 20% load.

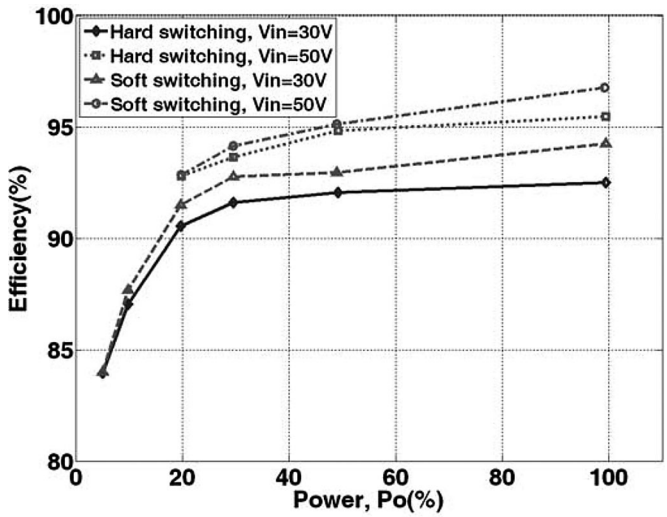

Fig. 14. Efficiency of $V_o = 380$ V.

the European efficiency was improved from 91.3% to 92.4% due to the ZVS operation under the $V_{\rm in} = 30$ V condition.

IV. Conclusion

This paper proposed a nonisolated ZVT two-inductor boost converter using a single resonant inductor for high step-up applications. Since the two main switches operate with ZVS, switching loss and diode reverse-recovery loss are reduced.

Furthermore, simple implementation and reduced size are possible due to the use of a single resonant inductor. Although variable switching frequency control must be utilized for the output-voltage regulation of the proposed converter under light load conditions at $V_{\text{in}} = 50$ V, the system efficiency is improved over a wide range of loads. The experimental results demonstrate that the proposed ZVT two-inductor converter is an excellent candidate for use in high step-up applications.

REFERENCES

[1] S. B. Kjær, J. K. Pedersen, and F. Blaabjerg, "A review of single-phase grid-connected inverters for photovoltaic modules," *IEEE Trans. Ind. Appl.*, vol. 41, no. 5, pp. 1292–1306, Sep./Oct. 2005.

[2] Q. Li and P. Wolfs, "A review of the single phase photovoltaic module integrated converter topologies with three different dc link configurations," *IEEE Trans. Power Electron.*, vol. 23, no. 3, pp. 1320–1333, May 2008.

[3] J.-S. Lai, "Power conditioning circuit topologies," *IEEE Ind. Electron. Mag.*, vol. 3, no. 2, pp. 24–34, Jun. 2009.

[4] W. H. Li, X. D. Lv, Y. Deng, J. Liu, and X. N. He, "A review of non-isolated high step-up dc/dc converters in renewable energy applications," in *Proc. 24th Annu. IEEE Appl. Power Electron. Conf. Exposition*, Washington, DC, Feb. 15–19, 2009, pp. 364–369.

[5] R. J. Wai and R.-Y. Duan, "High step-up converter with coupled-inductor," *IEEE Trans. Power Electron.*, vol. 20, no. 5, pp. 1025–1035, Sep. 2004.

[6] R.-J. Wai, C.-Y. Lin, R.-Y. Duan, and Y.-R. Chang, "High-efficiency dc-dc converter with high voltage gain and reduced switch stress," *IEEE Trans. Ind. Electron.*, vol. 54, no. 1, pp. 354–364, Feb. 2007.

[7] P. J. Wolfs, "A current-sourced dc–dc converter derived via the duality principle from the half-bridge converter," *IEEE Trans. Power Electron.*, vol. 40, no. 1, pp. 139–144, Feb. 1993.

[8] W. Li, J. Liu, J. Wu, and X. He, "Design and analysis of isolated ZVT boost converters for high-efficiency and high-step-up applications," *IEEE Trans. Power Electron.*, vol. 22, no. 6, pp. 2363–2373, Nov. 2007.

[9] L. Yan and B. Lehman, "An integrated magnetic isolated two-inductor boost converter: Analysis, design, and experimentation," *IEEE Trans. Power Electron.*, vol. 20, no. 2, pp. 332–342, Mar. 2005.

[10] H. L. Do, "A soft-switching dc/dc converter with high voltage gain," *IEEE Trans. Power Electron.*, vol. 25, no. 5, pp. 1193–1200, May 2010.

[11] S.-S. Lee, S.-W. Rhee, and G.-W. Moon, "Coupled inductor incorporated boost half-bridge converter with wide ZVS operation range," *IEEE Trans. Ind. Electron.*, vol. 56, no. 7, pp. 2505–2512, Jul. 2009.

[12] L. Po-Wa, L. Yim-Shu, D. K. W. Cheng, and L. Xiu-Cheng, "Steady-state analysis of an interleaved boost converter with coupled inductors," *IEEE Trans. Ind. Electron.*, vol. 47, no. 4, pp. 787–795, Aug. 2000.

[13] X. Huang, X. Wang, T. Nergaard, J. S. Lai, X. Xu, and L. Zhu, "Parasitic ringing and design issues of digitally controlled high power interleaved boost converters," *IEEE Trans. Power Electron.*, vol. 19, no. 5, pp. 1341–1352, Sep. 2004.

[14] Y.-C. Hsieh, T.-C. Hsueh, and H.-C. Yen, "An interleaved boost converter with zero-voltage transition," *IEEE Trans. Power Electron.*, vol. 24, no. 4, pp. 973–978, Apr. 2009.

[15] Q. Li and P. Wolfs, "An analysis of the ZVS two-inductor boost converter under variable frequency operation," *IEEE Trans. Power Electron.*, vol. 22, no. 1, pp. 120–131, Jan. 2007.

[16] S. J. Jang, C. Y. Won, B. K. Lee, and J. Hur, "Fuel cell generation system with a new active clamping current-fed half-bridge converter," *IEEE Trans. Energy Convers.*, vol. 22, no. 2, pp. 332–340, Jun. 2007.

[17] J. M. Kwon and B. H. Kwon, "High step-up active-clamp converter with input-current doubler and output-voltage doubler for fuel cell power systems," *IEEE Trans. Power Electron.*, vol. 24, no. 1, pp. 108–115, Jan. 2009.

[18] Y. Jang and M. M. Jovanovic, "New two-inductor boost converter with auxiliary transformer," *IEEE Trans. Power Electron.*, vol. 19, no. 1, pp. 169–175, Jan. 2004.

[19] N.-J. Park and D.-S. Hyun, "IBC using a single resonant inductor for high-power applications," *IEEE Trans. Ind. Electron.*, vol. 56, no. 5, pp. 1522–1530, May 2009.

[20] R. W. Erickson and D. Maksimović, *Fundamentals of Power Electronics*. Norwell, MA: Kluwer, 2001.

[21] L. A. Flores, O. García, A. Román, F. Rizo, and L. E. Arámbula, "Isolated two-inductor boost converter start-up and steady-state operation with any output voltage," in *Proc. Electron., Robot. Automotive Mech. Conf.*, 2007, pp. 639–644.

Kui-Jun Lee received the B.S. and M.S. degrees in electrical engineering from Hanyang University, Seoul, Korea, in 2005 and 2007, respectively, where he is currently working toward the Ph.D. degree.

His research interests include power converter system for renewable energies and soft switching techniques.

Byoung-Gun Park received the B.S. degree from Myongji University, Yongin, Korea, in 2005, and the M.S. and Ph.D. degrees from Hanyang University, Seoul, Korea, in 2007 and 2011, respectively, all in electrical engineering.

Since 2011, he has been with Korea Electrotechnology Research Institute, where he is currently a Senior Researcher in the Electric Motor Research Center. His research interests include motor drives, fault tolerant control, and power converter systems for electric vehicles.

Rae-Young Kim (S'06–M'10) received the B.S. and M.S. degrees from the Hanyang University, Seoul, Korea, in 1997 and 1999, respectively, and the Ph.D. degree from the Virginia Polytechnic Institute and State University, Blacksburg, VA, in 2009, all in electrical engineering.

From 1999 to 2004, he was a Senior Researcher at the Hyosung Heavy Industry R&D Center, Seoul. In 2009, he was a Post-Doctoral Researcher at National Semiconductor Corporation, engaged on a smart home energy management system. Since 2010, he has been with the Hanyang University, where he is currently an Assistant Professor in the Department of Electrical and Biomedical Engineering. His research interests include modeling and control of power converter systems, soft switching techniques, energy management systems in smart grid applications, power converter systems for renewable energies, and motor drive systems.

Dr. Kim received the First Prize Paper Award in Industry Applications Society (IAS) 2007. Since 2009, he has been a member of the IEEE IAS Industry Power Converters Committee, and also served as a Reviewer for the IEEE Transaction on Industrial Electronics and the IEEE Transaction on Industry Applications.

Dong-Seok Hyun (S'79–M'83–SM'91–F'03) received the B.S. and M.S. degrees in electrical engineering from Hanyang University, Seoul, Korea, in 1973 and 1978, respectively, and the Ph.D. degree in electrical engineering from Seoul National University, Seoul, Korea, in 1986.

From 1976 to 1979, he was a Researcher at the Agency of Defense Development, Daejeon, Korea. He was a Research Associate in the Department of Electrical Engineering, University of Toledo, Toledo, OH, from 1984 to 1985, and a Visiting Professor in the Department of Electrical Engineering, Technical University of Munich, Munich, Germany, from 1988 to 1989. Since 1979, he has been with Hanyang University, Seoul, Korea, where he is currently a Professor in the Department of Electrical Engineering and the Director of the Advanced Institute of Electrical Engineering and Electronics (AIEE). He is the author of more than 650 publications concerning electric machine design, high-power engineering, power electronics, and motor drives. His research interests include power electronics, motor drives, traction, and their control systems.

Dr. Hyun is a member of the IEEE Power Electronics, Industrial Electronics, Industry Applications, and Electron Devices Societies. He is also a member of the Institution of Engineering and Technology (IET), the Korean Institute of Power Electronics, and the Korean Institute of Electrical Engineers.